



Inhibition of the urea-urease reaction by the components of the zeolite imidazole frameworks-8 and the formation of urease-zinc-imidazole hybrid compound

Norbert Német¹ · Ylenia Miele² · Gábor Shusztér³ · Eszter L. Tóth¹ · János Andre Maróti⁴ · Péter János Szabó⁴ · Federico Rossi⁵ · István Lagzi^{1,6}

Received: 13 October 2021 / Accepted: 13 December 2021
© The Author(s) 2022

Abstract

In the past decade, much effort has been devoted to using chemical clock-type reactions in material design and driving the self-assembly of various building blocks. Urea-urease enzymatic reaction has chemical pH clock behavior in an unbuffered medium, in which the induction time and the final pH can be programmed by the concentrations of the reagents. The urea-urease reaction can offer a new alternative in material synthesis, where the pH and its course in time are crucial factors in the synthesis. However, before using it in any synthesis method, it is important to investigate the possible effects of the reagents on the enzymatic reaction. Here we investigate the effect of the reagents of the zeolite imidazole framework-8 (zinc ions and 2-methylimidazole) on the urea-urease reaction. We have chosen the zeolite imidazole framework-8 because its formation serves as a model reaction for the formation of other metal–organic frameworks. We found that, besides the inhibition effect of the zinc ions which is well-known in the literature, 2-methylimidazole inhibits the enzymatic reaction as well. In addition to the observed inhibition effect, we report the formation of a hybrid urease-zinc-2-methylimidazole hybrid material. To support the inhibition effect, we developed a kinetic model which reproduced qualitatively the experimentally observed kinetic curves.

Keywords Clock reaction · Inhibition · Urea-urease reaction · Material design

Introduction

A clock reaction (or chemical clock) is a type of chemical reaction in which the product appears suddenly with a well-defined time lag after starting the reaction [1–3]. The lag time is also defined as Landolt time after the iodine clock reaction

✉ István Lagzi
lagzi.istvan.laszlo@ttk.bme.hu

Extended author information available on the last page of the article

discovered by Heinrich Landolt [4]. Strictly speaking, a clock reaction is a two-step process with the time scale separation of the reactions ($A + \dots \rightarrow P + \dots$ with slow kinetics, $B + P \rightarrow \dots$ with fast kinetics and the initial concentration of A should be greater than that of the B) [2]. Chemical reactions with different kinetic and mechanistic features can also have an induction period, e.g., autocatalytic reactions ($A + P \rightarrow 2P$), consecutive reactions ($A \rightarrow B \rightarrow P$) and enzymatic reactions.

In recent years, the application of systems exhibiting chemical clock type behavior in the material design and driving the self-assembly of various building blocks has gained much attention. A key engineering issue is that the clock time (induction period) and the final concentration of the product (e.g., H^+) can be easily adjusted by the initial concentration of the reagents and experimental conditions (e.g., temperature) [5–9]. Predominantly reactions showing chemical clock type of behavior are based on reactive inorganic compounds (e.g., sulfite, bromate) and non-biocompatible reagents (e.g., formaldehyde). Due to this disadvantage, the application of these chemical clock-type systems involving bio-related components had been missing. Therefore, there was an increasing demand to develop biocompatible clock reactions to use in various bio-related applications. Enzymatic reactions can serve as possible candidates to overcome the previously mentioned drawbacks.

Because of their bell-shaped activity dependence on pH, certain enzymatic reactions can produce chemical clock type behavior in unbuffered media, if one or more products of the reaction itself affect the pH. One of the simplest systems showing such behavior is the hydrolysis of urea mediated by the enzyme urease to yield ammonia and carbon dioxide [10–12]. Urea-urease set was successfully employed for time programming of self-regulating supramolecular hydrogels [13, 14], spatiotemporal control of the gelation and polymerization fronts [15], layered compartmentalization [16] and vesicles self-division [17–19]. In material science, the urease reaction can be further employed to control the formation process of those compounds which synthesis relies on pH-sensitive precursors.

Metal–organic frameworks (MOFs) are unique porous crystalline materials having various applications in catalysis, gas storage and separation, electronics, chromatography, and drug delivery. [20–26] MOFs are usually produced by the coordination of metal cations and organic linkers in a liquid phase. The most common solvent in the solvothermal synthesis of MOFs is dimethylformamide (DMF). However, several protocols have been published on the generation of MOFs in the water phase. In this case, the strategy includes the application of the proper excess of the organic linkers and appropriately set pH to provide successful coordination to the metal cations [27–29].

Our ultimate goal is to use the bio-compatible urea-urease reaction in the synthesis of MOFs [30]. We hypothesize that the final pH and temporal change of the pH might significantly affect the morphology of the produced materials. However, before the design steps would be made it is crucial to investigate the effect of the reagents of MOFs on the kinetics of the enzymatic reaction. Here we investigate the effect of the components of the zeolite imidazole framework-8 (ZIF-8), zinc ions and 2-methylimidazole on the urea-urease reaction. We have chosen ZIF-8 because it serves as a model system for other MOFs and its formation has been extensively studied in the literature [31–36]. This type of investigation can be very important

since metal cations (as one reagent of MOFs) acts as inhibitors in the most enzymatic reaction [37–39]. In addition to this, we report the formation of a hybrid urease-zinc-2-methylimidazole (U-Zn-Met) structure.

Experimental

Urea ($\text{CO}(\text{NH}_2)_2$, Sigma), Urease enzyme from *Canavalia ensiformis* (Jack bean) (typically 40,150 units/g, Sigma-Aldrich), 2-methylimidazole (Sigma-Aldrich), zinc acetate dihydrate (Sigma-Aldrich), and acetic acid (CH_3COOH , Sigma-Aldrich) were used as received without further purification. The aqueous solutions of all chemicals (except acetic acid solution) were freshly prepared before each measurement, and the urease stock solution was stored at $\sim 8^\circ\text{C}$.

Kinetic experiments without the turbidity measurements were carried out in an open water-jacketed glass cell ($V = 22\text{ mL}$, $20.0 \pm 0.2^\circ\text{C}$), and the pH was monitored by a glass microelectrode (Mettler Toledo). The solutions of the reactants (with a total reaction volume of 18 mL) were consecutively added to the cell as follows: urea solution, 2-methylimidazole solution, acetic acid solution (to adjust the pH to ~ 4), zinc acetate solution, and urease solution. The reaction mixture was stirred by using a magnetic stirrer at 300 rpm.

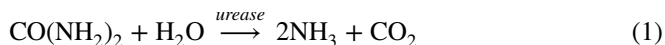
Kinetic experiments with the turbidity measurements were carried out in a cuvette with 10 cm optical path length and 100 mL volume. The cuvette was thermostated at $20.0 \pm 0.2^\circ\text{C}$ in a metal block with gaps for the light beam. The experimental procedure was similar to the kinetic experiments performed in a glass cell except that the turbidity was monitored by a UV–Vis spectrophotometer (VWR UV-1600PC) in kinetic mode ($\lambda = 600\text{ nm}$) connected to PC (Fig. S1 in the Supplementary Information, SI).

The formed white precipitate was filtered by using a $0.45\ \mu\text{m}$ syringe filter (cellulose-acetate) and washed three times with 3 mL distilled water and once with 2 mL DMF. Then the filter was dried ($\sim 24\text{ h}$), and the white precipitate was removed from the surface of the filter. The microstructure of the dried samples was characterized by scanning electron microscopy (SEM), the sample was transferred to the carbon tape and sputter-coated with gold.

Simulations

Numerical simulations were run by solving the ordinary differential equations corresponding to the kinetics of the chemical reactions involved in the process.

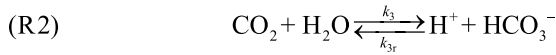
The urea-urease reaction has the general stoichiometry



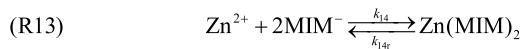
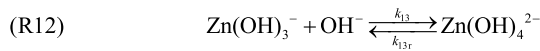
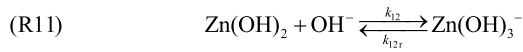
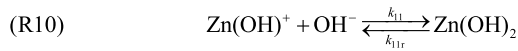
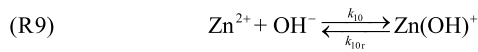
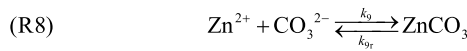
and the corresponding reaction rate is described by the Michaelis–Menten kinetics.

$$(RE) \quad R = \frac{v_{\max}[S]}{\left(K_M + [S]\left(1 + \frac{[S]}{K_S}\right)\right)\left(1 + \frac{[P]}{K_P}\right)\left(1 + \frac{K_{es2}}{[H^+]} + \frac{[H^+]}{K_{es1}}\right)},$$

Here $v_{\max} = k_1[E]$, with $[E]$ expressed as enzyme activity (units/mL), K_M is the Michaelis constant, K_{es1} and K_{es2} are protonation equilibrium constants of the substrate-enzyme complex. K_{es2} accounts for the dependence of the rate on the formation of an active protonated form of the enzyme-substrate complex (ESH, S is the substrate and EH the enzyme) and K_{es1} for the formation of an inactive biprotonated form (ESH $^{2+}$). $[P]$ is the concentration of the protonated form of ammonia (NH $_4^+$), $[S]$ is the concentration of urea, and K_S and K_P are the equilibrium constants for uncompetitive substrate and product inhibition, respectively. The pH is governed by the following equilibria



Here HA is acetic acid, MIMH is 2-methylimidazole, MIMH $_2^+$ is the protonated form of MIMH and MIM $^-$ is the deprotonated form. When Zn $^{2+}$ is added to the solution, several species can be generated according to the following equilibria



The set of ordinary differential equations derived from the reaction rates (reported in the SI) was numerically integrated by using the software XPPAUT [40] and COPASI [41] with the parameters listed in Tables S1–S3 in the SI.

Results and discussion

The urea-urease reaction yields carbon dioxide and ammonia (Eq. 1) and since stoichiometrically twice ammonia is produced than carbon dioxide, the pH continuously increases in an unbuffered medium [42]. In experiments, the initial pH of the reaction mixture was set to pH~4 by acetic acid, and due to the bell-shaped activity dependence of the enzyme on pH (having a maximum at pH=8.2 [12]) a sigmoidal kinetic curve (pH versus time) can be obtained. Figure 1a shows typical kinetic curves obtained in the urea-urease enzymatic reaction, it can be seen that the clock time ranges between ~30 and ~200 s in the excess substrate (urea) depending on the enzyme concentration. The inhibition effect of metal cations (especially zinc ions) on the urea-urease reaction is known and thoroughly explored [43–45], therefore, we did not investigate it in this study. On the other hand, no studies have been conducted on the effect of 2-methylimidazole on urease enzyme activity. Figures 1b and S2 show that the 2-methylimidazole significantly affects the enzymatic reaction. The activity of the enzyme was found to decrease up to ~70% when the concentration of the 2-methylimidazole was 100 mM (Fig. S2 in the SI), consequently the clock time increased, and it was found to be between 1000 and 3500 s at a fixed concentration of 2-methylimidazole (30.0 mM). The inhibition effect by the zinc ions and 2-methylimidazole can be explained by considering the same framework. In fact, the urease is a nickel-containing metalloenzyme, therefore, Zn^{2+} ions compete with Ni^{2+} in coordinating the protein groups thus changing the original enzymatic structure and affecting the activity. Since 2-methylimidazole coordinates with zinc ions (as a product of the ZIF-8), we can speculate a competition with protein groups to coordinate the nickel in the enzyme. Similarly, this coordination can affect the original active site geometry thus decreasing the enzyme activity.

First, we explored the cumulative inhibition effect of the reagents of the ZIF-8, and due to their pronounced effect on the urease activity, we carried out our kinetic investigation at low concentrations of zinc ions (1.0 mM) and 2-methylimidazole

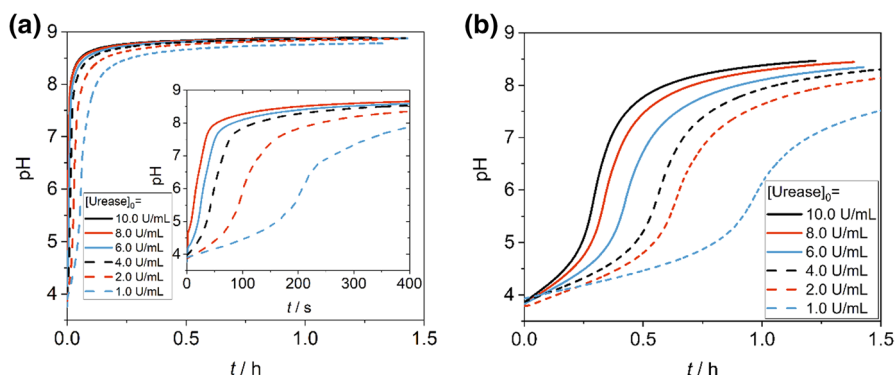


Fig. 1 pH kinetic curves of the urea-urease clock reactions with different enzyme concentrations in a batch reactor in the absence ($[\text{2-methylimidazole}]_0 = 0.0$ mM) **(a)** and the presence of 2-methylimidazole ($[\text{2-methylimidazole}]_0 = 30.0$ mM), **b** $[\text{urea}]_0 = 390$ mM and $[\text{CH}_3\text{COOH}]_0 = 80.9$ mM. The curves corresponding to 10.0 and 8.0 U mL^{-1} are overlapped in the inset

(4.0 mM) keeping only a slight excess of the organic linker. In these kinetic experiments, we recorded both the turbidity of the solution and the pH course. Fig. 2a, b show the kinetic curves (pH vs time) and Fig. 2c, d show variation of the turbidity in time in the case of fixed substrate concentration while the concentration of the enzyme was varied, and vice versa, when the enzyme concentration was fixed the urea concentration was changed. It can be seen that by increasing both the substrate and the enzyme concentrations the clock time (the interval between the start of the experiment and the time at which the rate of the pH change is maximum) is reduced. The enzyme concentration affects the final pH of the systems at the excess of the urea.

In all the experiments, when the pH reached ~ 6.4 , a white precipitate appeared in the solution causing an increase of turbidity as shown in Fig. 2c and d. After reaching the maximum value, the turbidity decreased in time due to the formation of bigger aggregates. We carried out several control experiments to investigate the origin of the precipitation phenomenon. First, we titrated a solution of zinc ions ($[\text{Zn}^{2+}]_0 = 1.0 \text{ mM}$) with the sodium hydroxide solution starting from $\text{pH} \sim 4$ similarly to the experiments with the enzyme, substrate, and linker. Zinc hydroxide appeared in the solution at $\text{pH} = 7.34$ indicating that the white precipitate cannot

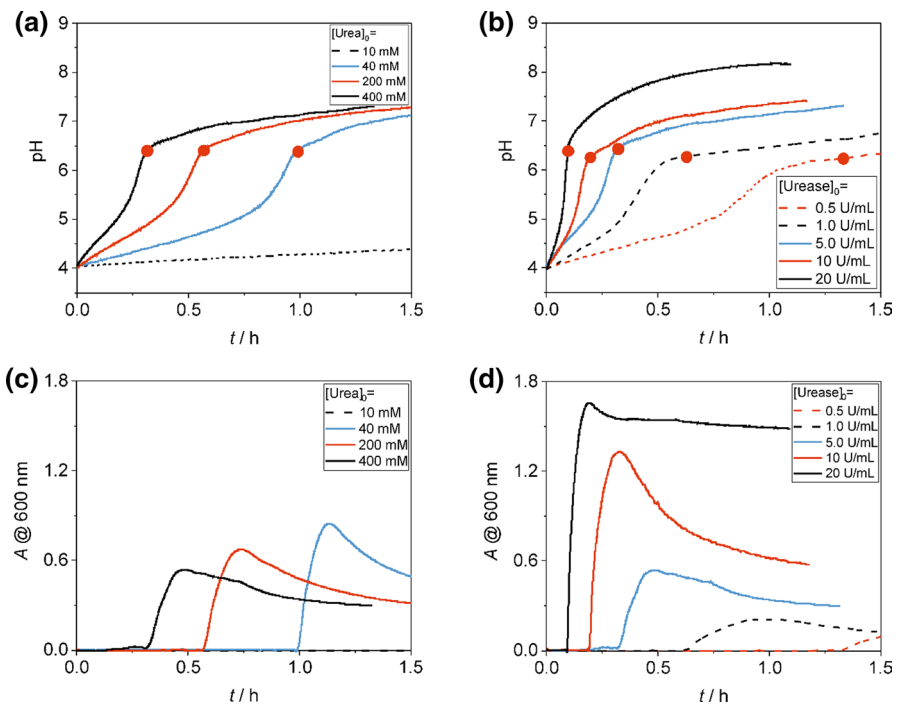


Fig. 2 Urea-urease reactions in the presence of $[\text{Zn}^{2+}] = 1 \text{ mM}$ and $[2\text{-methyl imidazole}] = 4 \text{ mM}$ with different urea (a) and (c) (where $[\text{urease}]_0 = 5 \text{ Unit/mL}$) and urease (b) and (d) (where $[\text{urea}]_0 = 400 \text{ mM}$) concentrations. The initial pH was set to 4 with an acetic acid solution. Red dots show when the turbidity started to increase from zero

be the zinc hydroxide because in most cases in the enzymatic reaction the final pH could not reach this value (Fig. S3a in the SI). Second round of the control experiments was the titration of a solution having zinc ions, 2-methylimidazole, and urease (in the absence of urea) with the sodium hydroxide solution starting from pH ~4 ($[\text{Zn}^{2+}]_0 = 1.0 \text{ mM}$, $[\text{2-methylimidazole}]_0 = 4.0 \text{ mM}$, and $[\text{urease}]_0 = 10.0 \text{ U/mL}$). In this case, we detected a turbidity change in the solution at pH = 6.07 (Fig. S3b in the SI). In the third setup, we titrated a solution having zinc ions, 2-methylimidazole, and urea (in the absence of urease) and observed no precipitation ($[\text{Zn}^{2+}]_0 = 1.0 \text{ mM}$, $[\text{2-methylimidazole}]_0 = 4.0 \text{ mM}$, and $[\text{urea}]_0 = 4.0 \text{ mM}$, Fig. S3c in the SI). We then hypothesized that the origin of the precipitation event could be attributed to the interaction of zinc ions with the enzyme. Therefore, we carried out control experiments titrating a solution of zinc ions and enzyme with the sodium hydroxide solution ($[\text{Zn}^{2+}]_0 = 1.0 \text{ mM}$ and $[\text{urease}]_0 = 10.0 \text{ U/mL}$). We observed the formation of a white precipitate accompanied by the increase of the turbidity at pH = 6.08 (Fig. S3d in the SI). Based on these control experiments, we could rule out the formation of either zinc hydroxide or ZIF-8 because the generated increase of pH was not high enough to facilitate their formation. However, we observed the precipitation of zinc ions with urease.

Numerical simulations can help to understand the behavior of urease in the presence of the ZIF-8 reactants. Figure 3 reports the integration of the ordinary differential equations describing the chemical equilibria (RE) and (R1)–(R7), in the presence and the absence of 2-methylimidazole. Figure 3a shows an excellent matching of the model with the experimental behavior of the urea hydrolysis in the absence of 2-methylimidazole when different amounts of the enzyme are added to the solution (integration parameters and kinetic constants are reported in Table S1 of the SI). To introduce the inhibitory effect of 2-methylimidazole, the kinetic constants $K_{\text{es}1}$ and $K_{\text{es}2}$, accounting for the pH dependency of the enzyme activity, were

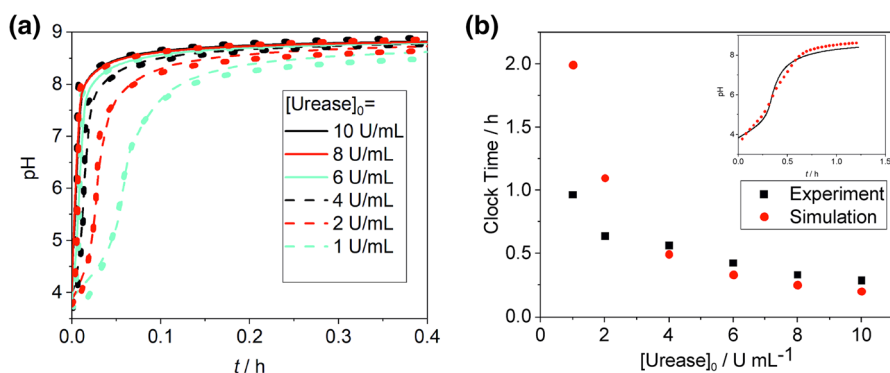


Fig. 3 Results of the numerical simulations of the urea-urease system. **a** Kinetic curves in the absence of 2-methylimidazole ($[\text{2-methylimidazole}]_0 = 0 \text{ mM}$) and comparison with the experimental results; dotted lines correspond to the simulations. **b** Simulated clock time in the presence of 2-methylimidazole ($[\text{2-methylimidazole}]_0 = 30.0 \text{ mM}$), the inset reports an example of simulated curve when $[\text{E}]_0 = 8 \text{ U/mL}$, $[\text{urea}]_0 = 390 \text{ mM}$, and $[\text{CH}_3\text{COOH}]_0 = 80.9 \text{ mM}$; solid and dotted lines corresponds to the experimental and numerical results, respectively. Kinetic constants and simulation parameters are reported in the SI

slightly decreased, while K_p , accounting for the non-competitive product inhibition, was increased (see details in Table S2 in the SI). Moreover, the basic character of 2-methylimidazole affects the final pH of the solution, as described by equilibria (R6) and (R7). As an example, the inset in Fig. 3b shows that the sigmoidal shape of the enzymatic reaction ($[\text{urea}]_0 = 390 \text{ mM}$, $[\text{CH}_3\text{COOH}]_0 = 80.9 \text{ mM}$, $[\text{E}]_0 = 8 \text{ U/mL}$, $[\text{2-methylimidazole}]_0 = 30.0 \text{ mM}$) is well described by the modified model, though with some deviations in the autocatalytic part and the trend of both the clock time (Fig. 3b) and the final pH of the solution (Fig. S4 in SI) at increasing $[\text{E}]_0$ is reproduced with a quantitative matching at high enzyme concentration.

When the zinc is added to the solution, additional chemical equilibria R8–R13 were included in the model through the corresponding kinetics (constants and parameters reported in Table S3 in the SI), but we could reproduce the general trends reported in Fig. 2 only by drastically changing the enzymatic kinetic constants and the concentration of some reactants. A possible explanation for the mismatch between experimental conditions and model parameters can be found in the formation of the precipitate, which can have multiple effects on global dynamics. As previously mentioned, Zn^{2+} itself is a strong inhibitor for the enzyme, in addition to this, when the enzyme is embedded in the precipitate, the diffusion of the substrate towards the active sites is strongly hindered. The net result would be that the real concentration of reactive urea is much lower than the theoretical one, as it happens when urease is loaded on resin particles [12]. In amino resin particles, the bell shape is shifted to lower pH values and the stability of the enzyme is increased. The values of $K_{\text{es}1}$, $K_{\text{es}2}$ and K_p change due to electrostatic interactions between the enzyme and the amino groups of the resin. Similarly, in our system, we observe a shift of the maximum activity towards lower pHs. This shift can depend on the interactions between Zn^{2+} and 2-methylimidazole with Ni^{2+} ions and the amino acids of the active site of urease.

At present we do not have enough data to account for reliable values of the kinetics constants, however, Fig. 4 shows that the experimental trend reported in Fig. 2b of the final pH (Fig. 4a) and of the clock time (Fig. 4b) with respect to the variation

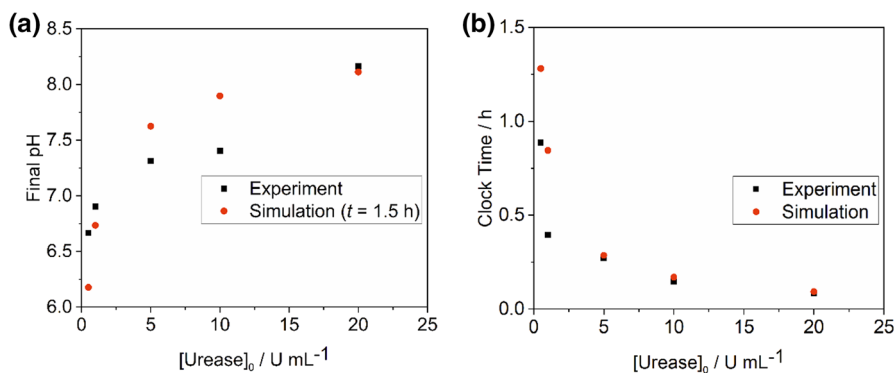


Fig. 4 Simulated final pH (a) and simulated clock time (b) for a system containing $[\text{Zn}^{2+}] = 1 \text{ mM}$, $[\text{2-methyl imidazole}] = 4 \text{ mM}$, $[\text{Urea}]_0 = 400 \text{ mM}$ and $[\text{HA}] = 1 \text{ mM}$ for different $[\text{Urease}]_0$

of $[E]_0$ can be simulated by decreasing of 2 orders of magnitude K_{es1} and increasing K_{es2} of 3 orders of magnitude. In contrast, data reported in Fig. 2a cannot be reproduced by our model, unless the concentrations of urea are decreased by 2 orders of magnitude.

To characterize the morphology of the precipitates, we performed scanning electron microscopy (SEM) measurements, and to increase the amount of the precipitate in experiments, we increased the concentration of zinc ions to 3.0 mM, but the ratio of the concentrations of the cation and linker remained 1:4. In the enzymatic reaction in the presence of zinc ions and linker, we obtained highly monodisperse spherical particles with an average size and polydispersity index (PDI) of 0.82 μm and 0.026, respectively (Fig. 5a). This morphology significantly differs from the crystal structures of the Zn^{2+} -enzyme compound (Fig. 5b—plate-like structure) and ZIF-8 crystals (Fig. 5c—dodecahedra). We exclude the encapsulation of the enzyme by ZIF-8 because, in this case, the morphology of the MOF crystals remained intact [46–48]. We hypothesize the following mechanism for the formation of the U-Zn-Met structure. When the pH increases driven by the urea-urease reaction, first the Zn^{2+} -enzyme compound is formed, which acts as heterogeneous nuclei for the further coprecipitation of the enzyme, Zn^{2+} , and 2-methylimidazole even in the pH range where no pure ZIF-8 formation is expected.

It should be noted that we cannot rule out the formation of zinc carbonate since the enzymatic system generates carbon dioxide which transforms into carbonate ions at alkaline conditions. Metal cations can react with carbonate ions producing carbonate precipitate. This strategy has been used in the remediation of heavy metals [49]. To investigate the formation of zinc carbonate, we carried out a control experiment in which zinc ions were titrated by a concentrated carbonate solution (Fig. S5 in the SI). We found that the zinc carbonate started to precipitate at $\text{pH} \sim 7.2$, which is higher than the pH for the appearance of the precipitate in the system ($\text{pH} \sim 6.4$, Fig. 2a and b). In other words, the observed precipitation is not due to the formation of the zinc carbonate.

We investigated the enzymatic activity of the formed precipitate (see the protocol in the SI). After each cycle, the U-Zn-Met was filtered, washed three times with distilled water, and redispersed in a liquid phase. Figure 6 shows that the activity of this hybrid compound gradually decreased until the third cycle in which the sample practically lost its enzymatic activity, which can be attributed to the disintegration of the structure.

Conclusions

In this study, we investigated the inhibition of 2-methylimidazole and the components of the ZIF-8 (zinc ions and 2-methylimidazole) in the urea-urease enzymatic reaction. We found that not only the zinc ions inhibit the reaction, but 2-methylimidazole does the same. Using the urea-urease enzymatic reaction, in the presence of the zinc cations and linker, we could not achieve the formation of ZIF-8 crystals due to the lower pH increase in the inhibited enzymatic reaction. We observed the formation of a hybrid U-Zn-Met material with a strong

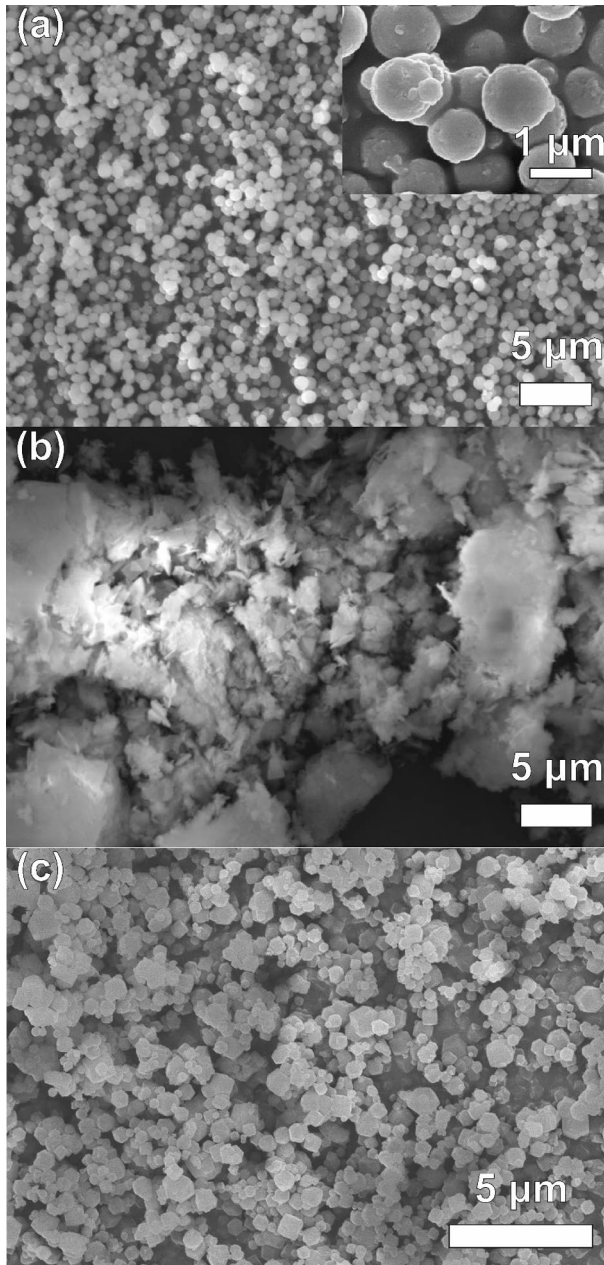
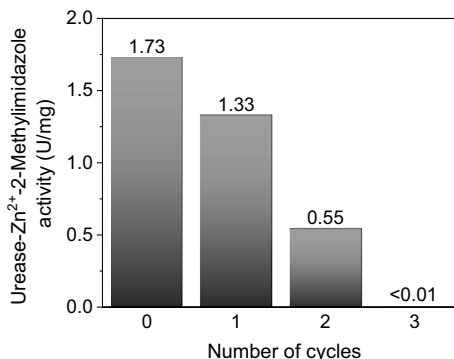


Fig. 5 SEM micrographs of precipitates formed in the urea-urease enzymatic reaction in the presence of the zinc ions and linker ($[\text{Zn}^{2+}]_0 = 3.0 \text{ mM}$, $[\text{2-methylimidazole}]_0 = 12.0 \text{ mM}$, $[\text{urea}]_0 = 390 \text{ mM}$, and $[\text{urease}]_0 = 10.0 \text{ U/mL}$) (a); zinc-urease crystals formed in the titration experiment with the solution of sodium hydroxide ($[\text{Zn}^{2+}]_0 = 3.0 \text{ mM}$, and $[\text{urease}]_0 = 10.0 \text{ U/mL}$) (b); ZIF-8 crystals in the direct reaction of zinc ions and linker ($[\text{Zn}^{2+}]_0 = 3.0 \text{ mM}$, $[\text{2-methylimidazole}]_0 = 12.0 \text{ mM}$) (c)

Fig. 6 Activity of the synthesized U-Zn-Met in several cycles. 0 corresponds to the initial activity of the U-Zn-Met calculated based on the concentration of the urease used



interaction between urease and the MOF reactants, Zn^{2+} and 2-methylimidazole, which was confirmed from the kinetic simulations. The kinetic model includes the pH equilibria, the enzymatic constants of the urea-urease system and the equilibria coming from the Zn^{2+} ions. The equilibria correlated to the formation of various zinc hydroxides, the precipitation of Zn carbonate and the ZIF formation (at pH higher than 10) do not affect significantly the final pH and the induction period for a wide range of values (even six orders of magnitude). The change of some enzymatic parameters (K_{es1} , K_{es2} and K_p) leads to a shift of the bell shape towards acidic pHs and better reproduces the experimental data (e.g., the sigmoidal shape with a low final pH). This trend is in line with the kinetic activity of other immobilized enzymes which are more stable and work even at lower pH values compared to the free enzyme. In future research, our aim would be to characterize this hybrid structure and understand if other chemical species of the enzymatic reaction are whether embedded in the structure.

Supplementary Information The online version contains supplementary material available at <https://doi.org/10.1007/s11144-021-02139-w>.

Acknowledgements This work was supported by the National Research, Development and Innovation Office of Hungary (K131425 and K119795) and the NRD Fund (TKP2020 IES, Grant No. BME-IE-NAT) based on the charter of bolster issued by the NRD Office under the auspices of the Ministry for Innovation and Technology.

Funding Open access funding provided by Budapest University of Technology and Economics.

Open Access This article is licensed under a Creative Commons Attribution 4.0 International License, which permits use, sharing, adaptation, distribution and reproduction in any medium or format, as long as you give appropriate credit to the original author(s) and the source, provide a link to the Creative Commons licence, and indicate if changes were made. The images or other third party material in this article are included in the article's Creative Commons licence, unless indicated otherwise in a credit line to the material. If material is not included in the article's Creative Commons licence and your intended use is not permitted by statutory regulation or exceeds the permitted use, you will need to obtain permission directly from the copyright holder. To view a copy of this licence, visit <http://creativecommons.org/licenses/by/4.0/>.

References



1. Horváth AK, Nagypál I (2015) Classification of clock reactions. *ChemPhysChem* 16:588–594. <https://doi.org/10.1002/cphc.201402806>
2. Lente G, Bazsa G, Fábíán I (2007) What is and what isn't a clock reaction? *New J Chem* 31:1707. <https://doi.org/10.1039/B708846A>
3. Limpanuparb T, Ruchawapol C, Sathainthammanee D (2019) Clock reaction revisited: catalyzed redox substrate-depletive reactions. *J Chem Educ* 96:812–818. <https://doi.org/10.1021/acs.jchemed.8b00547>
4. Landolt H (1886) Ueber die Zeitdauer der Reaction zwischen Jodsäure und schwefliger Säure. *Ber Dtsch Chem Ges* 19:1317–1365
5. Heuser T, Steppert AK, Molano LC, Zhu B, Walther A (2015) Generic concept to program the time domain of self-assemblies with a self-regulation mechanism. *Nano Lett* 15:2213–2219. <https://doi.org/10.1021/nl5039506>
6. Heinen L, Walther A (2015) Celebrating Soft Matter's 10th anniversary: approaches to program the time domain of self-assemblies. *Soft Matter* 11:7857–7866. <https://doi.org/10.1039/C5SM01660F>
7. Tóth-Szeles E, Horváth J, Holló G, Szűcs R, Hideyuki N, Lagzi I (2017) Chemically coded time-programmed self-assembly. *Mol Syst Des Eng* 2:274–282. <https://doi.org/10.1039/C7ME00020K>
8. Tóth-Szeles E, Medveczky Z, Holló G, Horváth J, Szűcs R, Hideyuki N, Lagzi I (2018) pH mediated kinetics of assembly and disassembly of molecular and nanoscopic building blocks. *React Kinet Mech Cat* 123:323–333. <https://doi.org/10.1007/s1144-017-1312-x>
9. Riedel S, Schweizer T, Smith-Mannschott K, Dufresne ER, Panzarasa G (2021) Supramolecular gelation controlled by an iodine clock. *Soft Matter* 17:1189–1193. <https://doi.org/10.1039/D0SM02285C>
10. Hu G, Pojman JA, Scott SK, Wrobel MM, Taylor AF (2010) Base-catalyzed feedback in the urea–urease reaction. *J Phys Chem B* 114:14059–14063. <https://doi.org/10.1021/jp106532d>
11. Bubanja IN, Bánsági T, Taylor AF (2018) Kinetics of the urea–urease clock reaction with urease immobilized in hydrogel beads. *React Kinet Mech Cat* 123:177–185. <https://doi.org/10.1007/s1144-017-1296-6>
12. Yang D, Fan J, Cao F, Deng Z, Pojman JA, Ji L (2019) Immobilization adjusted clock reaction in the urea–urease–H⁺ reaction system. *RSC Adv* 9:3514–3519. <https://doi.org/10.1039/C8RA09244C>
13. Heuser T, Weyandt E, Walther A (2015) Biocatalytic feedback-driven temporal programming of self-regulating peptide hydrogels. *Angew Chem Int Edit* 54:13258–13262. <https://doi.org/10.1002/anie.201505013>
14. Panja S, Adams DJ (2021) Urea-urease reaction in controlling properties of supramolecular hydrogels: pros and cons. *Chem-Eur J* 27:8928–8939. <https://doi.org/10.1002/chem.202100490>
15. Jee E, Bánsági T, Taylor AF, Pojman JA (2016) Temporal control of gelation and polymerization fronts driven by an autocatalytic enzyme reaction. *Angew Chem Int Ed* 55:2127–2131. <https://doi.org/10.1002/anie.201510604>
16. Fan X, Walther A (2021) Autonomous transient pH flips shaped by layered compartmentalization of antagonistic enzymatic reactions. *Angew Chem Int Ed* 60:3619–3624. <https://doi.org/10.1002/anie.202009542>
17. Miele Y, Holló G, Lagzi I, Rossi F (2021) Effect of the membrane composition of giant unilamellar vesicles on their budding probability: a trade-off between elasticity and preferred area difference. *Life* 11:634. <https://doi.org/10.3390/life11070634>
18. Holló G, Miele Y, Rossi F, Lagzi I (2021) Shape changes and budding of giant vesicles induced by an internal chemical trigger: an interplay between osmosis and pH change. *Phys Chem Chem Phys* 23:4262–4270. <https://doi.org/10.1039/D0CP05952H>
19. Miele Y, Medveczky Z, Holló G, Tegze B, Derényi I, Hórvölgyi Z, Altamura E, Lagzi I, Rossi F (2020) Self-division of giant vesicles driven by an internal enzymatic reaction. *Chem Sci* 11:3228–3235. <https://doi.org/10.1039/C9SC05195C>
20. Furukawa H, Cordova KE, O'Keefe M, Yaghi OM (2013) The chemistry and applications of metal-organic frameworks. *Science* 341:1230444. <https://doi.org/10.1126/SCIENCE.1230444>
21. Gascon J, Corma A, Kapteijn F, Llabrés i Xamena FX (2014) Metal organic framework catalysis: Quo vadis? *ACS Catal* 4:361–378. <https://doi.org/10.1021/cs400959k>

22. Rosi NL, Eckert J, Eddaoudi M, Vodak DT, Kim J, O'Keeffe M, Yaghi OM (2003) Hydrogen storage in microporous metal-organic frameworks. *Science* 300:1127–1129. <https://doi.org/10.1126/science.1083440>
23. Adams R, Carson C, Ward J, Tannenbaum R, Koros W (2010) Metal organic framework mixed matrix membranes for gas separations. *Micropor Mesopor Mat* 131:13–20. <https://doi.org/10.1016/j.micromeso.2009.11.035>
24. Campbell M, Dincă M (2017) Metal–organic frameworks as active materials in electronic S sensor devices. *Sensors* 17:1108. <https://doi.org/10.3390/s17051108>
25. Han S, Wei Y, Valente C, Lagzi I, Gassensmith JJ, Coskun A, Stoddart F, Grzybowski BA (2010) Chromatography in a single metal–organic framework (MOF) crystal. *J Am Chem Soc* 132:16358–16361. <https://doi.org/10.1021/ja1074322>
26. Zheng H, Zhang Y, Liu L, Wan W, Guo P, Nyström AM, Zou X (2016) One-pot synthesis of metal–organic frameworks with encapsulated target molecules and their applications for controlled drug delivery. *J Am Chem Soc* 138:962–968. <https://doi.org/10.1021/jacs.5b11720>
27. He M, Yao J, Liu Q, Wang K, Chen F, Wang H (2014) Facile synthesis of zeolitic imidazolate framework-8 from a concentrated aqueous solution. *Micropor Mesopor Mat* 184:55–60. <https://doi.org/10.1016/j.micromeso.2013.10.003>
28. Choi HS, Lee SJ, Bae YS, Choung SJ, Im SH, Kim J (2015) Scalable continuous solvo-jet process for ZIF-8 nanoparticles. *Chem Eng J* 266:56–63. <https://doi.org/10.1016/j.cej.2014.12.068>
29. Kolmykov O, Commenge JM, Alem H, Giroit E, Mozet K, Medjahdi G, Schneider R (2017) Microfluidic reactors for the size-controlled synthesis of ZIF-8 crystals in aqueous phase. *Mater Design* 122:31–41. <https://doi.org/10.1016/j.matdes.2017.03.002>
30. Liang W, Wied P, Carraro F, Sumbly CJ, Nidetzky B, Tsung CK, Falcaro P, Doonan CJ (2021) Metal–organic framework-based enzyme biocomposites. *Chem Rev* 121:1077–1129. <https://doi.org/10.1021/acs.chemrev.0c01029>
31. Lee YR, Jang MS, Cho HY, Kwon HJ, Ahn WS (2015) ZIF-8: A comparison of synthesis methods. *Chem Eng J* 271:276–280. <https://doi.org/10.1016/j.cej.2015.02.094>
32. Pan Y, Liu Y, Zeng G, Zhao L, Lai Z (2011) Rapid synthesis of zeolitic imidazolate framework-8 (ZIF-8) nanocrystals in an aqueous system. *Chem Commun* 47:2071. <https://doi.org/10.1039/C0CC05002D>
33. Chen B, Yang Z, Zhu Y, Xia Y (2014) Zeolitic imidazolate framework materials: recent progress in synthesis and applications. *J Mater Chem A* 2:16811–16831. <https://doi.org/10.1039/C4TA02984D>
34. Li K, Miwornunyuie N, Chen L, Jingyu H, Amaniampong PS, Koomson DA, Ewusi-Mensah D, Xue W, Li G, Lu H (2021) Sustainable application of ZIF-8 for heavy-metal removal in aqueous solutions. *Sustainability* 13:984. <https://doi.org/10.3390/su13020984>
35. Wang Q, Sun Y, Li S, Zhang P, Yao Q (2020) Synthesis and modification of ZIF-8 and its application in drug delivery and tumor therapy. *RSC Adv* 10:37600–37620. <https://doi.org/10.1039/D0RA07950B>
36. Zheng B, Sant M, Demontis P, Suffritti GB (2012) Force field for molecular dynamics computations in flexible ZIF-8 framework. *J Phys Chem C* 116:933–938. <https://doi.org/10.1021/jp209463a>
37. Carter EL, Flugga N, Boer JL, Mulrooney SB, Hausinger RP (2009) Interplay of metal ions and urease. *Metallomics* 1:207. <https://doi.org/10.1039/b903311d>
38. Larsen KS, Auld DS (1989) Carboxypeptidase A: mechanism of zinc inhibition. *Biochemistry* 28:9620–9625. <https://doi.org/10.1021/bi00451a012>
39. Yang Z, Liu S, Zheng D, Feng S (2006) Effects of cadmium, zinc and lead on soil enzyme activities. *J Environ Sc* 18:1135–1141. [https://doi.org/10.1016/S1001-0742\(06\)60051-X](https://doi.org/10.1016/S1001-0742(06)60051-X)
40. <http://www.math.pitt.edu/~bard/xpp/xpp.html>
41. Hoops S, Sahle S, Gauges R, Lee C, Pahle J, Simus N, Singhal M, Xu L, Mendes P, Kummer U (2006) COPASI—a COPASIM Pathway Simulator. *Bioinformatics* 22:3067–3074. <https://doi.org/10.1093/bioinformatics/btl485>
42. Krajewska B (2009) Ureasases I. functional, catalytic and kinetic properties: a review. *J Mol Catal B-Enzym* 59:9–21. <https://doi.org/10.1016/j.molcatb.2009.01.003>
43. Li Y, Xu L, Duan M, Zhang B, Wang Y, Guan Y, Wu J, Jing C, You Z (2019) Syntheses, characterization, crystal structures and Jack bean urease inhibitory activities of Zn^{II}, Co^{II/III} and Ni^{II} complexes derived from reduced Schiff base ligand. *Polyhedron* 166:146–152. <https://doi.org/10.1016/j.poly.2019.03.051>
44. Park IS, Hausinger RP (1996) Metal ion interactions with urease and ureD-urease apoproteins. *Biochemistry* 35:5345–5352. <https://doi.org/10.1021/bi952894j>

45. Shaw WHR, Raval DN (1961) The inhibition of urease by metal ions at pH 8.9. *J Am Chem Soc* 83:3184–3187. <https://doi.org/10.1021/ja01476a004>
46. Liang K, Coghlan CJ, Bell SG, Doonan C, Falcaro P (2016) Enzyme encapsulation in zeolitic imidazolate frameworks: a comparison between controlled co-precipitation and biomimetic mineralisation. *Chem Commun* 52:473–476. <https://doi.org/10.1039/C5CC07577G>
47. Liang K, Ricco R, Doherty CM, Styles MJ, Bell S, Kirby N, Mudie S, Haylock D, Hill AJ, Doonan CJ, Falcaro P (2015) Biomimetic mineralization of metal-organic frameworks as protective coatings for biomacromolecules. *Nat Commun* 6:7240. <https://doi.org/10.1038/ncomms8240>
48. Liang X, Li Q, Shi Z, Bai S, Li Q (2020) Immobilization of urease in metal–organic frameworks via biomimetic mineralization and its application in urea degradation. *Chin J Chem Eng* 28:2173–2180. <https://doi.org/10.1016/j.cjche.2020.01.014>
49. Bhattacharya A, Naik SN, Khare SK (2019) Efficacy of ureolytic *Enterobacter cloacae* EMB19 mediated calcite precipitation in remediation of Zn (II). *J Environ Sci Heal A* 54:536–542. <https://doi.org/10.1080/10934529.2019.1567184>

Publisher's Note Springer Nature remains neutral with regard to jurisdictional claims in published maps and institutional affiliations.

Authors and Affiliations

Norbert Németh¹ · Ylenia Miele² · Gábor Shuszter³  · Eszter L. Tóth¹ ·
János Endre Maróti⁴ · Péter János Szabó⁴ · Federico Rossi⁵  · István Lagzi^{1,6} 

¹ Department of Physics, Budapest University of Technology and Economics, Budafoki út 8, 1111 Budapest, Hungary

² Department of Chemistry and Biology “A. Zambelli”, University of Salerno, Via Giovanni Paolo II 132, 84084 Fisciano, SA, Italy

³ Department of Physical Chemistry and Materials Science, University of Szeged, Rerrich Béla tér 1, 6720 Szeged, Hungary

⁴ Department of Materials Science and Engineering, Budapest University of Technology and Economics, Budapest, Hungary

⁵ Department of Earth, Environmental and Physical Sciences—DEEP Sciences, University of Siena, Pian dei Mantellini 44, 53100 Siena, Italy

⁶ MTA-BME Condensed Matter Physics Research Group, Budafoki út 8, 1111 Budapest, Hungary